

Dynamic localization in optical lattices¹

Stephan Arlinghaus, Matthias Langemeyer, and Martin Holthaus²

May 28, 2018

¹Chapter 12 of the volume: **Dynamical Tunneling - Theory and Experiment**, edited by S. Keshavamurthy and P. Schlagheck (Taylor and Francis CRC, 2011)

²Carl von Ossietzky Universität
Institut für Physik
D - 26111 Oldenburg, Germany

Contents

- 1 Dynamic localization in optical lattices 1
- 1.1 The basic idea 2
- 1.2 Does it work? 7
- 1.3 What is it good for? 22

Chapter 1

Dynamic localization in optical lattices

The concept of dynamic localization goes back to an observation reported by Dunlap and Kenkre in 1986: The wave packet of a single particle moving on a single-band tight-binding lattice endowed with only nearest-neighbor couplings remains perpetually localized when driven by a spatially homogeneous ac force, provided the amplitude and the frequency of that force obey a certain condition [1]. When trying to overcome the limitations of the model, it is comparatively straightforward to deal with an arbitrary form of the dispersion relation — thus abandoning the nearest-neighbor approximation — and with arbitrary time-periodic forces, thus doing away with the restriction to purely sinusoidal driving [2]. But in any real lattice system an external time-periodic force will induce interband transitions, and it is by no means obvious whether dynamic localization can survive when these come into play.

In this chapter we consider ultracold atoms in driven optical lattices, which provide particularly attractive, experimentally well accessible examples of quantum particles in spatially periodic structures exposed to time-periodic forcing [3, 4, 5]. Such systems are much cleaner, and more easy to control, than electrons in crystal lattices under the influence of ac electric fields, for which the original idea had been developed [1]. With the help of results obtained

by numerical calculations we illustrate that such ultracold atoms in kHz-driven optical lattices exhibit dynamic localization in almost its purest form if the parameters are chosen judiciously, despite the potentially devastating presence of interband transitions.

When viewing dynamic localization as resulting from a band collapse [6, 7], far-reaching further possibilities emerge. Namely, the actual strength of deviations from exact spatial periodicity, be they isolated [8], random [9], or quasiperiodic [10, 11], is measured relative to the effective band width. Thus, when the band in question almost collapses in response to time-periodic driving, the effects of even slight deviations from exact lattice periodicity are strongly enhanced. This allows one, in particular, to coherently control the “metal-insulator”-like incommensurability transition occurring in sufficiently deep quasiperiodic optical lattices [10, 11, 12]. While the very transition has already been observed with Bose-Einstein condensates in bichromatic optical potentials [13], its coherent control by means of time-periodic forcing still awaits its experimental verification.

1.1 The basic idea

The one-dimensional tight-binding system described by the Hamiltonian

$$H_0 = -J \sum_{\ell} \left(|\ell + 1\rangle \langle \ell| + |\ell\rangle \langle \ell + 1| \right), \quad (1.1)$$

where $|\ell\rangle$ denotes a Wannier state localized at the ℓ th lattice site, and J is the hopping matrix element connecting neighboring sites, is about the simplest model for the formation of Bloch bands. Assuming that the unspecified number of sites is so large that finite-size effects may be neglected, its energy eigenstates are Bloch waves

$$|\varphi_k\rangle = \sum_{\ell} |\ell\rangle \exp(i\ell ka) \quad (1.2)$$

labeled by a wave number k ; the lattice period is given by a . The corresponding energy dispersion relation reads

$$E(k) = -2J \cos(ka); \quad (1.3)$$

here we assume $J > 0$, so that its minimum is located at $k = 0 \bmod 2\pi/a$. Now we let an external time-dependent, spatially homogeneous force $F(t)$ act on the system, such that the total Hamiltonian becomes

$$H(t) = H_0 + H_1(t) \quad (1.4)$$

with

$$H_1(t) = -F(t) \sum_{\ell} |\ell\rangle a \ell \langle \ell| . \quad (1.5)$$

It is easy to verify that the wave functions

$$|\psi_k(t)\rangle = \exp\left(-\frac{i}{\hbar} \int_0^t d\tau E(q_k(\tau))\right) \sum_{\ell} |\ell\rangle \exp(i\ell q_k(t)a) \quad (1.6)$$

then are solutions to the time-dependent Schrödinger equation, provided the time-dependent wave numbers $q_k(t)$ introduced here obey the “semiclassical” relation

$$\hbar \dot{q}_k(t) = F(t) . \quad (1.7)$$

We demand that $q_k(t)$ be equal to k at time $t = 0$, and therefore set

$$q_k(t) = k + \frac{1}{\hbar} \int_0^t d\tau F(\tau) . \quad (1.8)$$

These wave functions (1.6), originally considered by Houston in the context of crystal electrons exposed to a uniform electric field superimposed on a periodic lattice potential [14], are known as “accelerated Bloch waves”, or Houston states.

In the particular case of a monochromatic force with angular frequency ω and amplitude F_1 , given by

$$F(t) = F_1 \cos(\omega t) , \quad (1.9)$$

one has

$$q_k(t) = k + \frac{F_1}{\hbar\omega} \sin(\omega t) , \quad (1.10)$$

so that $q_k(t)$ naturally acquires the temporal period $T = 2\pi/\omega$ of the driving force. Then also $E(q_k(t))$ is T -periodic, but the Houston state (1.6) is not, because the integral appearing

in the exponential prefactor acquires a contribution which grows linearly with time. In order to extract that contribution, we calculate the one-cycle average

$$\begin{aligned}\varepsilon(k) &\equiv \frac{1}{T} \int_0^T d\tau E(q_k(\tau)) \\ &= -2J_{\text{eff}} \cos(ka) ,\end{aligned}\tag{1.11}$$

thus obtaining an effective hopping matrix element given by

$$J_{\text{eff}} = J J_0\left(\frac{F_1 a}{\hbar\omega}\right) ,\tag{1.12}$$

with $J_0(z)$ denoting the Bessel function of zero order. We then write

$$\exp\left(-\frac{i}{\hbar} \int_0^t d\tau E(q_k(\tau))\right) = \exp\left(-\frac{i}{\hbar} \int_0^t d\tau [E(q_k(\tau)) - \varepsilon(k)]\right) \exp\left(-i\varepsilon(k)t/\hbar\right) ,\tag{1.13}$$

so that the first exponential on the right hand side now is T -periodic by construction. Hence, for the T -periodic force (1.9) the Houston states (1.6) can be cast into a form

$$|\psi_k(t)\rangle = |u_k(t)\rangle \exp\left(-i\varepsilon(k)t/\hbar\right)\tag{1.14}$$

with T -periodic functions $|u_k(t)\rangle$,

$$|u_k(t)\rangle = |u_k(t+T)\rangle .\tag{1.15}$$

This leads to a remarkable conclusion. Any wave packet governed by the full Hamiltonian (1.4) with periodic forcing (1.9) can be expanded with respect to these states (1.14) with coefficients that are constant in time, because the time-dependence already is fully incorporated into the states themselves. After each cycle T the T -periodic functions $|u_k(t)\rangle$ are restored, so that the time evolution of the wave packet, when viewed stroboscopically at intervals T , is determined by the different “speed” of rotation of the complex phase factors $\exp(-i\varepsilon(k)t/\hbar)$ of the packet’s individual components. But if all quantities $\varepsilon(k)$ are equal, which according to Eqs. (1.11) and (1.12) occurs when the scaled driving amplitude

$$K_0 \equiv \frac{F_1 a}{\hbar\omega}\tag{1.16}$$

equals a zero of the Bessel function J_0 , all phase factors evolve at the same speed, so that the wave packet reproduces itself exactly after each period: There is some T -periodic wiggling, but no long-term motion. This, in short, is dynamic localization [1].

The above argument appears so special, and the decisive step (1.13) so swift, that it is not easy to see how to transfer this finding to more realistic situations: How can one incorporate deviations from exact lattice periodicity into this reasoning? How to proceed when several bands are coupled by interband transitions? The answer to these questions is provided by the Floquet picture, which does not directly take recourse to the spatial lattice periodicity, but rather builds on the temporal periodicity of the Hamiltonian: When $H(t) = H(t + T)$, there exists a complete set of solutions to the time-dependent Schrödinger equation of the particular form

$$|\psi_n(t)\rangle = |u_n(t)\rangle \exp(-i\varepsilon_n t/\hbar), \quad (1.17)$$

where the functions $|u_n(t)\rangle = |u_n(t + T)\rangle$ inherit the T -periodicity of the underlying Hamiltonian. These states are known as Floquet states; the quantities ε_n are dubbed as quasienergies [15, 16, 17, 18]. Obviously the Houston states (1.6) with time-periodic forcing are particular examples of such Floquet states; from now on we employ an abstract state label n instead of the wave number k in order to also admit settings without lattice periodicity. In the case of the Houston-Floquet states, the determination of their quasienergies (1.11) essentially was a by-product of the solution of an initial value problem. The general case, however, has to proceed along a more sophisticated route: Floquet states and quasienergies are determined by solving the eigenvalue problem

$$\left(H(t) - i\hbar \frac{\partial}{\partial t} \right) |u_n(t)\rangle = \varepsilon_n |u_n(t)\rangle, \quad (1.18)$$

posed in an *extended Hilbert space* of T -periodic functions; in that space time plays the role of a *coordinate*. Therefore, if $\langle u_1(t)|u_2(t)\rangle$ is the scalar product of two T -periodic functions in the usual physical Hilbert space, their scalar product in the extended space reads [18]

$$\langle\langle u_1|u_2\rangle\rangle \equiv \frac{1}{T} \int_0^T dt \langle u_1(t)|u_2(t)\rangle. \quad (1.19)$$

Hence, we write $|u_n(t)\rangle$ for a Floquet eigenfunction when viewed in the physical Hilbert

space, and $|u_n(t)\rangle\rangle$ when that same function is regarded as an element of the extended space.

A most important consequence of this formalism stems from the fact that when $|u_n(t)\rangle\rangle$ is a solution to the problem (1.18) with eigenvalue ε_n , then $|u_n(t)\exp(im\omega t)\rangle\rangle$ is a further solution with eigenvalue $\varepsilon_n + m\hbar\omega$, where we have set $\omega = 2\pi/T$, and m is any (positive, zero, or negative) integer, in order to comply with the required T -periodic boundary condition. For $m \neq 0$ these two solutions are orthogonal with respect to the scalar product (1.19). But when going back to the physical Hilbert space, one has

$$|u_n(t)\exp(im\omega t)\rangle\rangle \exp\left(-i(\varepsilon_n + m\hbar\omega)/\hbar\right) = |u_n(t)\rangle\rangle \exp(-i\varepsilon_n t/\hbar), \quad (1.20)$$

so that the two different solutions represent *the same* Floquet state (1.17). We conclude that a physical Floquet state does not simply correspond to an individual solution to the eigenvalue problem (1.18), but rather to a whole class of such solutions labeled by the state index n , whereas the “photon” index m distinguishes different representatives of such a class. Likewise, a quasienergy should not be regarded as a single eigenvalue, but rather as a set $\{\varepsilon_n + m\hbar\omega \mid m = 0, \pm 1, \pm 2, \dots\}$ associated with one particular state n , while m ranges through all integers. Therefore, each “quasienergy Brillouin zone” of width $\hbar\omega$ contains one quasienergy representative of each state.

The time evolution of any wave function can then be written as a Floquet-state expansion,

$$|\psi(t)\rangle\rangle = \sum_n c_n |u_n(t)\rangle\rangle \exp(-i\varepsilon_n t/\hbar), \quad (1.21)$$

where the coefficients c_n remain constant in time. This is one of the main benefits offered by the Floquet picture, and allows one to draw many parallels to the evolution of systems governed by a time-independent Hamiltonian.

Equipped with this set of tools, it is now clear how to investigate the possible occurrence of dynamic localization in realistic lattice structures: One has to solve the eigenvalue problem (1.18) for the Hamiltonian with the respective full lattice potential, and to enquire whether the resulting quasienergy bands collapse at least approximately, that is, acquire negligible widths for certain parameters. If so, any wave packet prepared in a quasienergy

band at a collapse point will suffer from “prohibited dephasing”, as in the archetypal model specified by Eqs. (1.1), (1.5), and (1.9); and thus remain dynamically localized. Interband transitions then are automatically included, with multiphoton-like resonances manifesting themselves through quasienergy-curve anticrossings [19].

In the following section we will carry through this program for ultracold atoms in driven one-dimensional optical lattices.

1.2 Does it work?

A one-dimensional optical lattice is created by two counterpropagating laser beams with wave number k_L , suitably detuned from a dipole-allowed transition of the atomic species moving in this standing light wave. By means of the ac Stark effect, the spatially periodic electric field experienced by the atoms then translates into a cosine potential

$$V_{\text{lat}}(x) = \frac{V_0}{2} \cos(2k_L x) \quad (1.22)$$

for their translational motion along the lattice, with a depth V_0 that is proportional to the laser intensity [20, 21]. The characteristic energy scale then is given by the single-photon recoil energy

$$E_{\text{rec}} = \frac{\hbar^2 k_L^2}{2M}, \quad (1.23)$$

where M denotes the atomic mass. To give a numerical example, when working with ^{87}Rb in a lattice generated by laser radiation with wavelength $\lambda = 2\pi/k_L = 842 \text{ nm}$ [4, 5] one has $E_{\text{rec}} = 1.34 \cdot 10^{-11} \text{ eV}$. Thus, typical lattice depths of 5 to 10 recoil energies are on the order of 10^{-10} eV — which means that one encounters many phenomena with ultracold atoms in optical lattices which are known from traditional solid-state physics, but scaled down in energy by no less than 10 orders of magnitude.

This also tells us what “ultracold” means. Taking an ensemble of atoms with a temperature T_{ens} such that $k_B T_{\text{ens}}$ is roughly equal to E_{rec} , say, where k_B is Boltzmann’s constant,

the de Broglie wavelength of these atoms, given by

$$\lambda_{\text{deBroglie}} = \frac{h}{\sqrt{2\pi M k_B T_{\text{ens}}}} \approx \frac{2}{\sqrt{\pi}} \frac{\lambda}{2}, \quad (1.24)$$

is barely longer than the lattice constant $a = \lambda/2$. But in order to experience quantum mechanical lattice effects, the particles have to be able to “feel” the periodic structure, so that $\lambda_{\text{deBroglie}}$ should cover *at least* a few lattice constants — which means that being this cold is not cold enough: We even require $k_B T_{\text{ens}} \ll E_{\text{rec}}$.

With hardly any thermal excitation energy left the atoms occupy only the lowest Bloch band of their optical lattice, so that the single-particle Hamiltonian with the lattice potential (1.22) translates directly into the single-band tight-binding model (1.1) when working in a basis of Wannier functions pertaining to that lowest band, and neglecting all couplings other than those between nearest neighbors, denoted as J . The accuracy of this approximation increases with increasing lattice depth [4, 12]: For $V_0/E_{\text{rec}} = 5$ the magnitude of the ratio of the neglected matrix element connecting next-to-nearest neighbors to J still reaches about 5%, but it decreases to about 1% when $V_0/E_{\text{rec}} = 10$. Moreover, when expressing the exact band structure of a cosine lattice in terms of characteristic values of the Mathieu equation, and noting that the width W of the cosine energy band (1.3) is $4J$, one finds the approximation [21]

$$J/E_{\text{rec}} \sim \frac{4}{\sqrt{\pi}} \left(\frac{V_0}{E_{\text{rec}}} \right)^{3/4} \exp \left(-2\sqrt{\frac{V_0}{E_{\text{rec}}}} \right) \quad \text{for } V_0/E_{\text{rec}} \gg 1. \quad (1.25)$$

The requisite still missing now is the time-periodic force corresponding to the model (1.5). This can be effectuated either by introducing a small oscillating frequency difference between the two lattice-generating laser beams, as detailed later, or by retro-reflecting one such beam off an oscillating mirror back into itself [3, 4, 5]. In a frame of reference co-moving with the oscillating lattice, one then obtains the single-particle Hamiltonian

$$H(t) = \frac{p^2}{2M} + V_{\text{lat}}(x) - F_1 x \cos(\omega t + \phi), \quad (1.26)$$

where p is the atomic center-of-mass momentum in the lattice direction, the driving force is

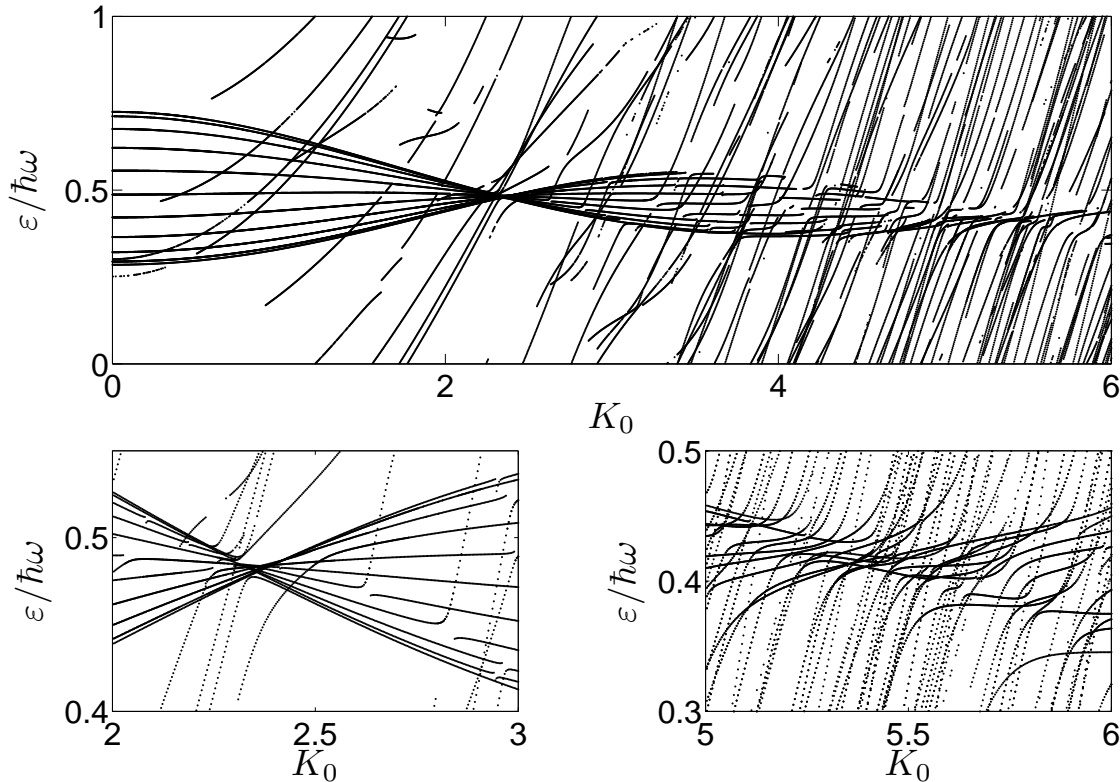


Figure 1.1: Above: One Brillouin zone of quasienergies for the optical lattice (1.22) with depth $V_0/E_{\text{rec}} = 5.7$, driven with scaled frequency $\hbar\omega/E_{\text{rec}} = 0.5$, vs. the scaled driving amplitude K_0 . The lower left panel testifies that the first band collapse is almost perfect, whereas the second one, enlarged in the lower right panel, is already thwarted by multiphoton-like resonances.

parametrized in accordance with Eq. (1.9), and we have also admitted an arbitrary phase ϕ .

In all our model calculations we consider a lattice with depth $V_0/E_{\text{rec}} = 5.7$, implying that the width of the lowest Bloch band is $W/E_{\text{rec}} = 0.22$, whereas the gap between this lowest band and the first excited one figures as $\Delta/E_{\text{rec}} = 2.76$. Even for such a comparatively shallow lattice, which is routinely being realized in current experiments [5], the dispersion of the lowest band already is reasonably well described by the tight-binding cosine approximation (1.3), setting $J = W/4$. In order to obtain dynamic localization, the driving frequency should then be chosen such that the quantum $\hbar\omega$ is significantly smaller than the gap Δ , so that, perturbatively speaking, interband transitions require higher-order multiphoton-like processes, which would be suppressed as long as the driving amplitude F_1

is not too strong [19]. On the other hand, it is reasonable to demand that $\hbar\omega$ be larger than the band width, so that the band fits into a single quasienergy Brillouin zone. A good choice of the driving frequency should therefore adhere to the chain $4J = W < \hbar\omega < \Delta$; we take $\hbar\omega/E_{\text{rec}} = 0.5$ in all numerical scenarios depicted below. For ^{87}Rb atoms in a lattice with $\lambda = 842$ nm this choice fixes the frequency at $\omega/(2\pi) = 1.62$ kHz.

Figure 1.1 shows one Brillouin zone of quasienergies for these parameters vs. the scaled driving amplitude K_0 , as defined by Eq. (1.16). Observe that the first quasimomentum Brillouin zone ranges from $-\hbar\pi/a = -\hbar k_{\text{L}}$ to $+\hbar\pi/a = +\hbar k_{\text{L}}$; the homogeneous force does not mix states with different wave numbers [10]. Hence, we combine quasienergies for states with $k = (i/10)k_{\text{L}}$ in this plot, with $i = 0, 1, 2, \dots, 10$. In this way, the comparison of the ideal quasienergy band (1.11) with the one appearing in the actual optical lattice is greatly facilitated. Evidently the first band collapse is almost perfect, although it is slightly shifted from $K_0 = 2.405$, the first zero of J_0 , to $K_0 \approx 2.35$. In contrast, the second collapse, expected at $K_0 = 5.520$, already is significantly affected by a host of anticrossings, indicating multiphoton-like resonances. Thus, with $V_0/E_{\text{rec}} = 5.7$ and $\hbar\omega/E_{\text{rec}} = 0.5$ we may expect almost perfect dynamic localization at the first collapse point, whereas there will be strong disturbances of the ideal dynamics at the second one.

In Fig. 1.2 we depict the lowest quasienergy band for $K_0 = 0$, where it coincides with the original energy band; $K_0 = 1.18$, where its width is reduced by a factor of $J_0(1.18) = 0.681$; and at the first collapse point, $K_0 = 2.35$. Ideally, a collapsed quasienergy band is completely flat, so that dynamic localization is associated with an infinite effective mass of the driven Bloch particle. Here we still observe some residual dispersion, probably resulting from both next-to-nearest neighbor couplings and couplings to higher bands, but the degree of band flattening achieved by the driving force is nonetheless impressive.

The ultimate demonstration of dynamic localization requires, of course, the inspection of wave-packet dynamics. To this end, we first compute the Bloch states $\langle x|\varphi_{1,k}\rangle$ of the lowest energy band of the lattice (1.22), and use them to design an initial wave packet

$$\langle x|\psi(t=0)\rangle = \int_{-k_{\text{L}}}^{k_{\text{L}}} dk g_1(k, t=0) \langle x|\varphi_{1,k}\rangle \quad (1.27)$$

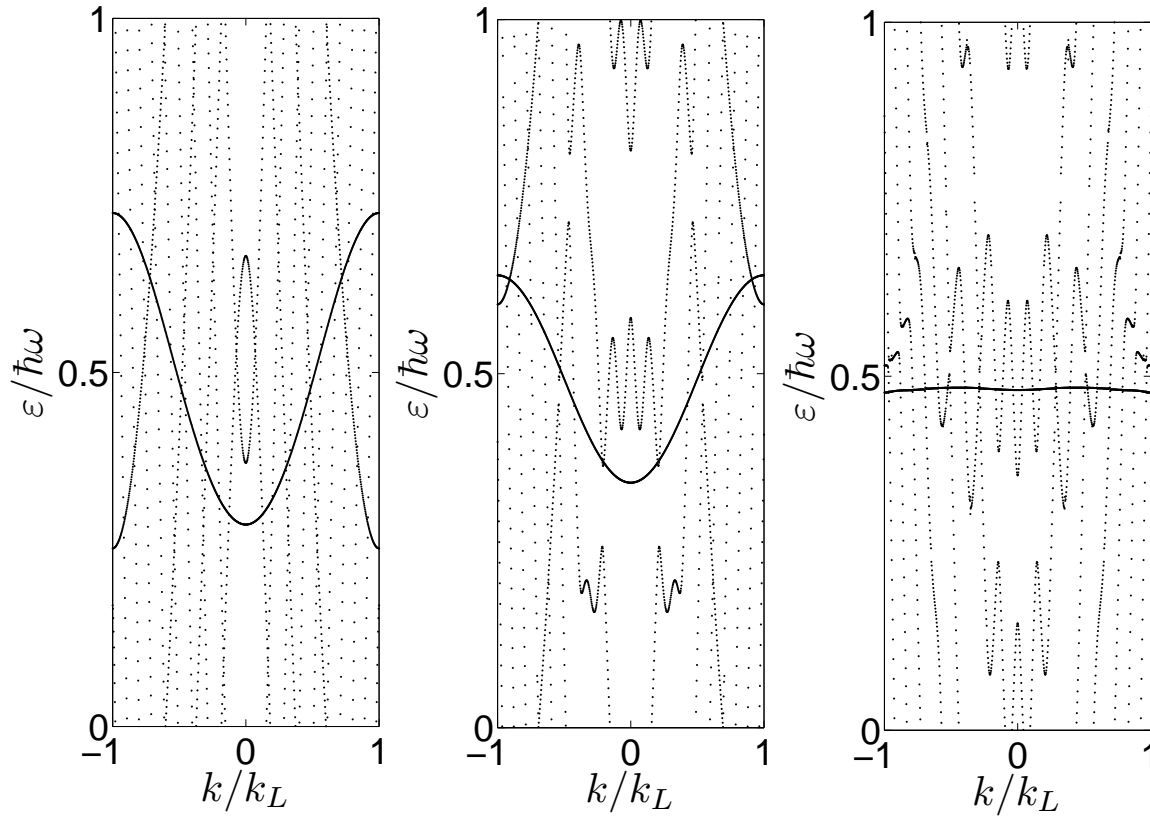


Figure 1.2: “Lowest” quasienergy band for the optical lattice (1.22) with depth $V_0/E_{\text{rec}} = 5.7$, driven with scaled frequency $\hbar\omega/E_{\text{rec}} = 0.5$, and scaled amplitudes $K_0 = 0$ (left), 1.18 (middle), and 2.35 (right). Additional curves result from higher bands.

with a Gaussian k -space distribution

$$g_1(k, t=0) = \frac{1}{\sqrt{2k_L\sqrt{\pi}\Delta k}} \exp\left(-\frac{(k - k_c)^2}{2(\Delta k)^2}\right) \quad (1.28)$$

centered around some predetermined wave number k_c , with width Δk . The corresponding probability density $|\langle x|\psi(t=0)\rangle|^2$ is concentrated in the wells of the lattice potential, equipped with a Gaussian envelope that varies the more slowly with x the narrower its distribution (1.28), that is, the smaller Δk . We then take this packet (1.27) as initial condition, and compute the wave function $\langle x|\psi(t)\rangle$ for $t > 0$ by solving the time-dependent Schrödinger equation numerically, fixing the phase ϕ in the Hamiltonian (1.26) at the value $\phi = \pi/2$. This means that the force $F(t) = F_1 \cos(\omega t + \phi)$ is instantaneously switched on at $t = 0$.

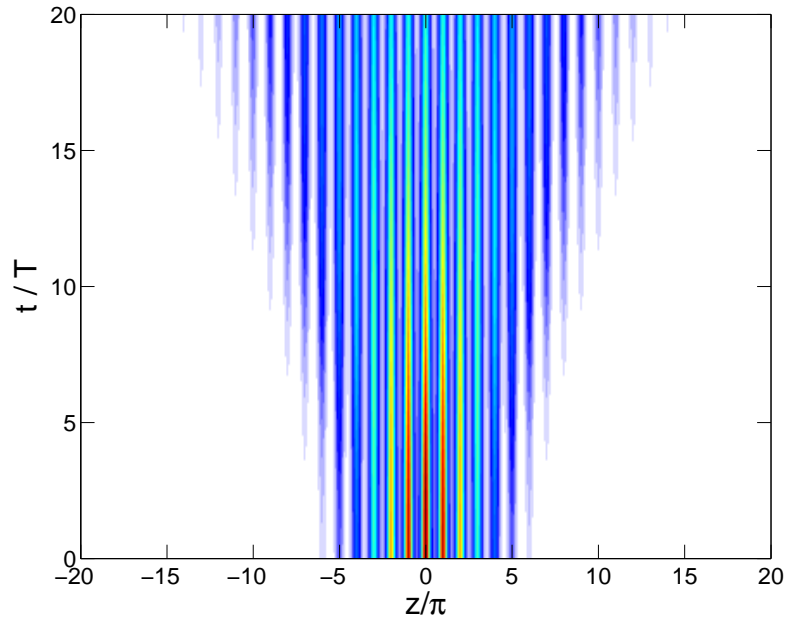


Figure 1.3: Spreading of the Bloch wave packet (1.27) with initial k -space width $\Delta k/k_L = 0.1$, and initial momentum $k_c/k_L = 0$, in the unforced optical lattice. In this and the following figures, density is encoded in shades of gray.

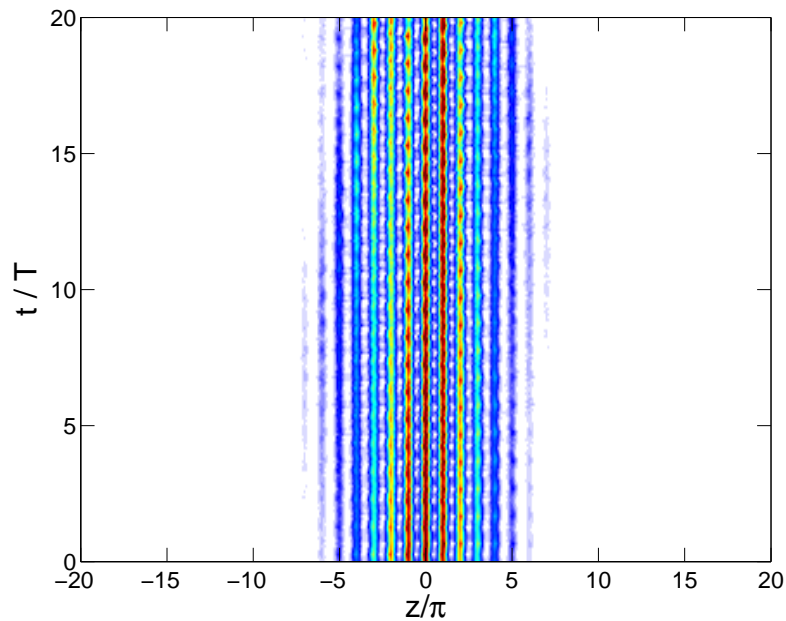


Figure 1.4: Evolution of the same initial wave packet as in Fig. 1.3 at the first band collapse ($K_0 = 2.35$): Here one encounters almost perfect dynamic localization; wave-packet spreading is disabled because the quasienergy band is dispersionless.

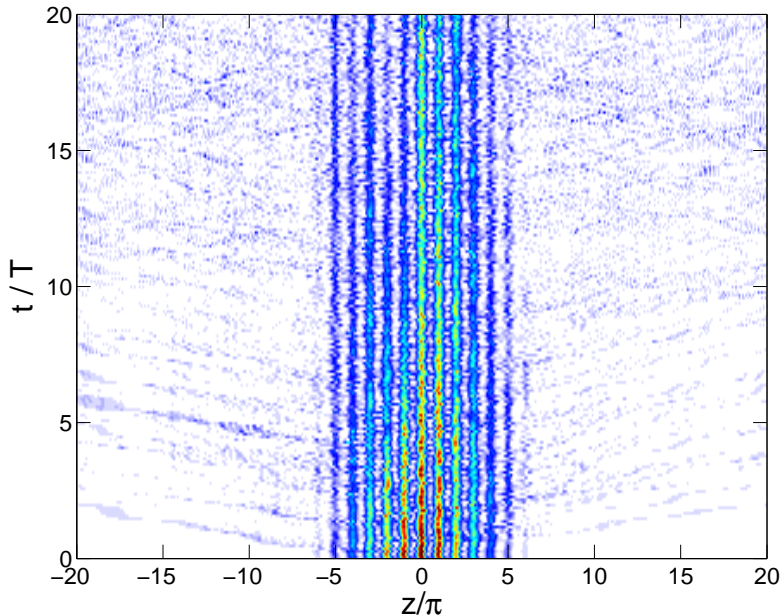


Figure 1.5: Evolution of the same initial wave packet as in Fig. 1.3 at the supposed second band collapse ($K_0 = 5.52$): Here the multiphoton-like resonances visible in Fig. 1.1 lead to a marked degradation of the localization.

Figure 1.3 shows a density plot of the wave packet when it evolves in the undriven lattice, that is, for $K_0 = 0$; the density is encoded in shades of gray. In this and the following figures, spatial extensions are measured in terms of the dimensionless coordinate $z = k_L x$, so that a distance $\Delta z/\pi = 1$ corresponds to one lattice period; moreover, the time scale is set by the period $T = 2\pi/\omega$. With $k_c/k_L = 0$ the initial packet carries no net momentum; its width is chosen as $\Delta k/k_L = 0.1$. As expected, the width of the packet then grows in the course of time by well-to-well tunneling.

In Fig. 1.4 we depict the density of the wave packet that evolves from the same initial condition when the driving amplitude is tuned to the first band collapse at $K_0 = 2.35$. Here we observe dynamic localization at its very best: The spreading has stopped, the packet is “frozen”.

It is then also of interest to monitor the evolution at the supposed second collapse, at $K_0 = 5.52$; this is done in Fig. 1.5. While the “regular spreading” that has been prominent in Fig. 1.3 indeed seems to have stopped, small probability wavelets leak out of the initial packet almost immediately, spreading rapidly over the lattice. This is an effect of the multiphoton-

like resonances previously spotted in Fig. 1.1, which assist parts of the wave function in getting to higher bands, allowing them to escape on a short time scale.

As long as interband transitions remain negligible, the resulting single-band dynamics can often be regarded as “semiclassical” [22]: Namely, if an initial packet is strongly centered in k -space around some arbitrary wave number $k_c \equiv k_c(0)$, this center wave number evolves in time according to Bloch’s famous “acceleration theorem”

$$\hbar \dot{k}_c(t) = F(t) , \quad (1.29)$$

similar to the evolution (1.7) of the index of a single Houston state. The model Hamiltonian (1.26) specifies $F(t) = F_1 \cos(\omega t + \phi)$, so that in this case

$$k_c(t) = k_c(0) + \frac{F_1}{\hbar\omega} \left(\sin(\omega t + \phi) - \sin(\phi) \right) . \quad (1.30)$$

The packet’s group velocity then is given by the derivative of the dispersion relation $E(k)$ of the band it lives in, evaluated at this moving center wave number (1.30):

$$v_{\text{group}}(t) = \left. \frac{1}{\hbar} \frac{dE}{dk} \right|_{k_c(t)} . \quad (1.31)$$

Taking the tight-binding relation (1.3) as a good approximation for the actual lowest energy band of our model, this yields

$$v_{\text{group}}(t) = \frac{2Ja}{\hbar} \sin(k_c(t)a) . \quad (1.32)$$

Upon time-averaging, one is therefore left with

$$\bar{v}_{\text{group}} = \frac{2J_{\text{eff}}a}{\hbar} \sin(k_c(0)a - K_0 \sin(\phi)) , \quad (1.33)$$

where J_{eff} again is the driving-dependent effective hopping matrix element (1.12), and K_0 is the scaled amplitude (1.16). Thus, the initial phase ϕ may be utilized for imparting some momentum to the packet. Nonetheless, for any combination of $k_c(0)$ and ϕ the average group velocity vanishes when $J_{\text{eff}} = 0$, as corresponding to ideal dynamic localization.

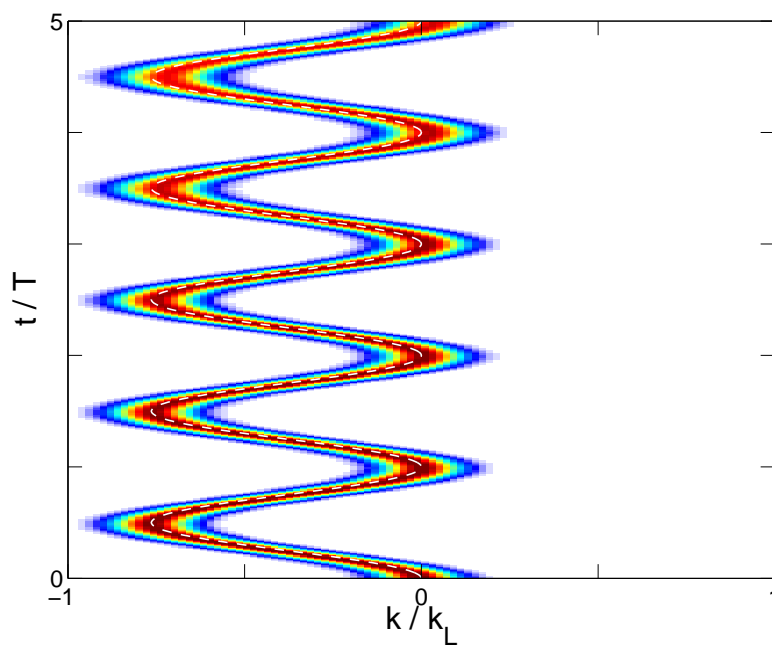


Figure 1.6: Evolution of the k -space distribution initially given by Eq. (1.28) with width $\Delta k/k_L = 0.1$, for $K_0 = 1.2$ and $k_c/k_L = 0$. The white-dashed line indicates the “classical” solution (1.30).

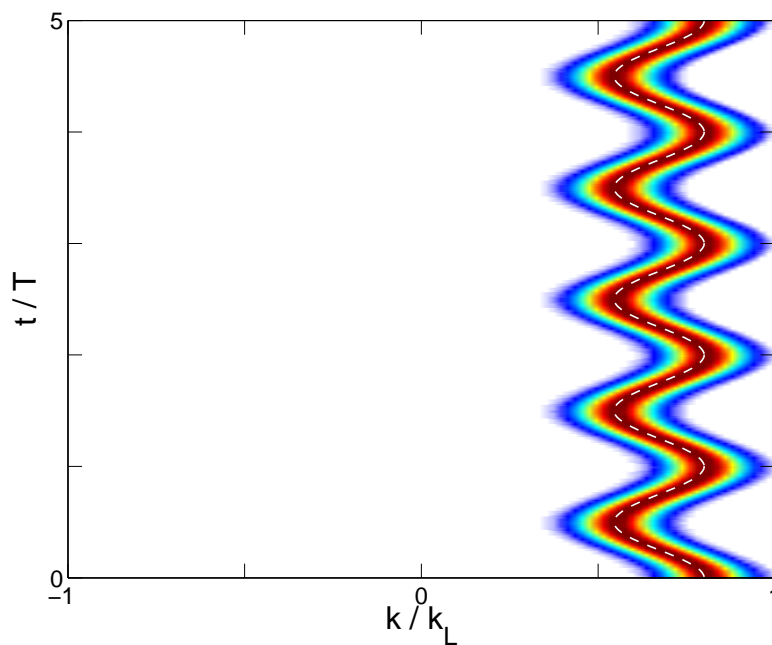


Figure 1.7: Evolution of the k -space distribution initially given by Eq. (1.28) with width $\Delta k/k_L = 0.1$, but now for $K_0 = 0.4$ and $k_c/k_L = 0.8$, so that the white-dashed “classical” solution (1.30) starts from a non-zero value.

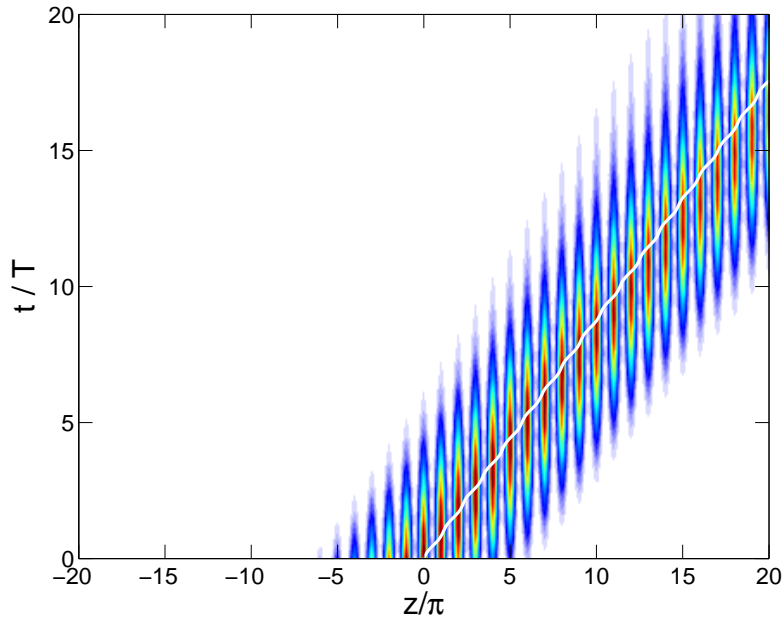


Figure 1.8: Evolution of the Bloch wave packet (1.27) with initial k -space width $\Delta k/k_L = 0.1$ and initial momentum $k_c/k_L = 0.8$, driven with scaled amplitude $K_0 = 0.4$, as corresponding to the k -space distribution depicted in Fig. 1.7. The white line marks the trajectory obtained by integrating the oscillating group velocity (1.32).

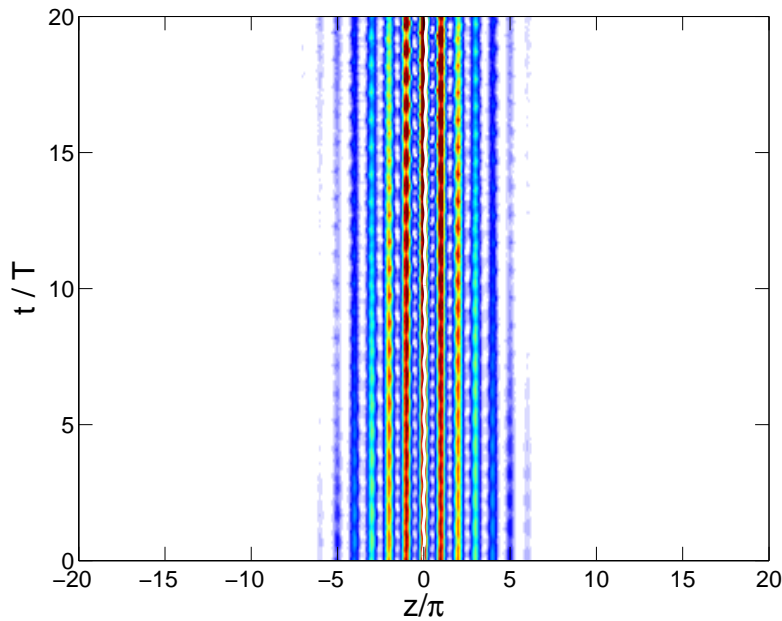


Figure 1.9: Evolution of the Bloch wave packet (1.27) with initial k -space width $\Delta k/k_L = 0.1$ and initial momentum $k_c/k_L = 0.8$, now driven with scaled amplitude $K_0 = 2.35$: Despite the nonzero average momentum, the average group velocity vanishes because of the band collapse. The white line in the center is obtained as described in Fig. 1.8.

This semiclassical behavior is illustrated by a further set of figures. In Fig. 1.6 we plot the evolution of the exact k -space density that originates from the initial condition (1.28). Again we set $\Delta k/k_L = 0.1$, meaning that the distribution is sufficiently narrow to ensure the validity of Eq. (1.31); moreover, $k_c/k_L = 0$ and $K_0 = 1.2$. Since $\phi = \pi/2$, the distribution then oscillates around $\bar{k} = -F_1/(\hbar\omega)$, or $\bar{k}/k_L = -K_0/\pi$, following precisely the k -space trajectory predicted by Eq. (1.30).

A nonzero average momentum of the packet can likewise be achieved by selecting some suitable value of k_c/k_L . Figure 1.7 shows an example with $k_c/k_L = 0.8$, while $K_0 = 0.4$ and $\Delta k/k_L = 0.1$. This obviously corresponds to a wave function $\langle x|\psi(t)\rangle$ which moves into the positive x -direction all the time; the density of this wave function is displayed in Fig. 1.8. Here the white line indicates the classical trajectory that results from integrating the group velocity (1.32); indeed, this trajectory describes the motion of the packet's center quite well. When adjusting the driving amplitude to the first collapse, as in Fig. 1.9, the average motion stops despite the nonzero average momentum, as it should; when increasing K_0 to still higher values, so that J_{eff} becomes negative, the packet's direction of motion can even be reversed.

While the semiclassical approach to dynamic localization may be helpful, insofar as it appeals to our intuition, its explanation in terms of “prohibited dephasing” resulting from a quasienergy band collapse is *much* more powerful: This view immediately reveals that not only does the average motion of a wave packet come to a complete standstill, but so does its spreading; moreover, prohibited dephasing applies to *any* initial condition, regardless whether or not its envelope varies sufficiently slowly to justify the semiclassical approximation. As an extreme example of “nonclassical” motion we consider in Fig. 1.10 the undriven evolution of a wave function that coincides with a single Wannier function of the optical lattice [12] at $t = 0$, and therefore certainly does not possess a slowly varying envelope then, giving rise to a fairly complex spreading pattern which differs substantially from the semiclassical one previously visualized in Fig. 1.3. Nonetheless, when driven with the amplitude $K_0 = 2.35$ marking the first quasienergy band collapse, one observes another occurrence of dynamic localization, as witnessed by Fig. 1.11; the difference between the two evolution patterns depicted in Figs. 1.10 and 1.11 could hardly be more striking.

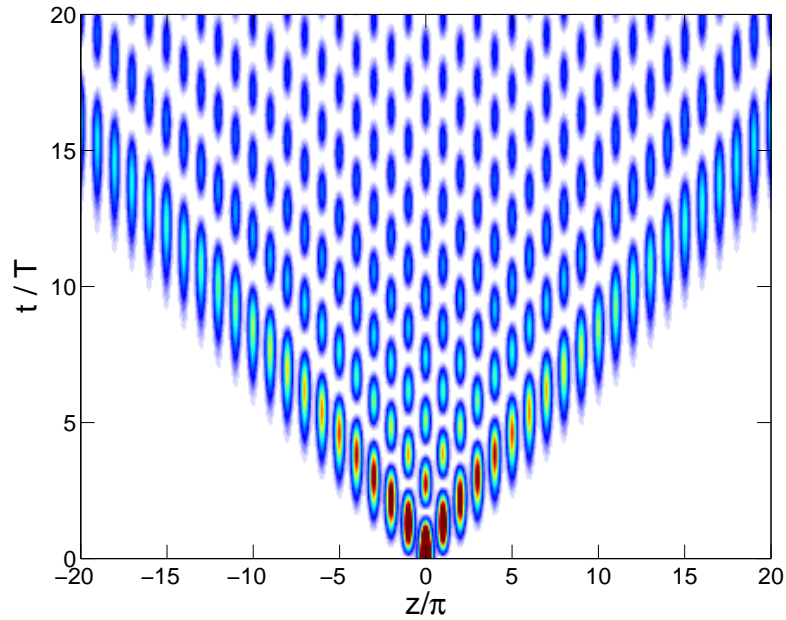


Figure 1.10: Evolution of the wave function that originates from an initial single Wannier state in the undriven lattice. This state does not possess a slowly varying envelope, and thus does not conform to semiclassical dynamics.

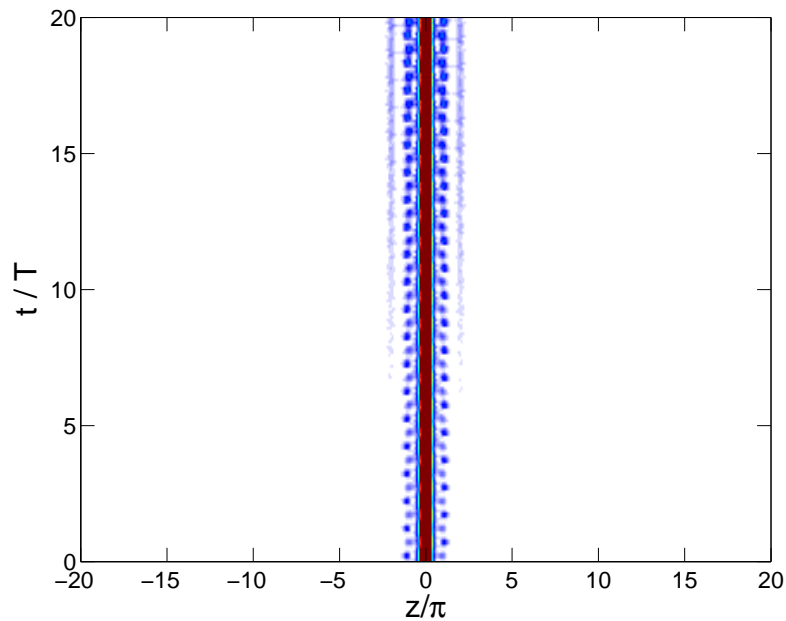


Figure 1.11: Evolution of the wave function that originates from an initial single Wannier state when driven with scaled amplitude $K_0 = 2.35$. The semiclassical approximation is not applicable here, but dynamic localization works nonetheless.

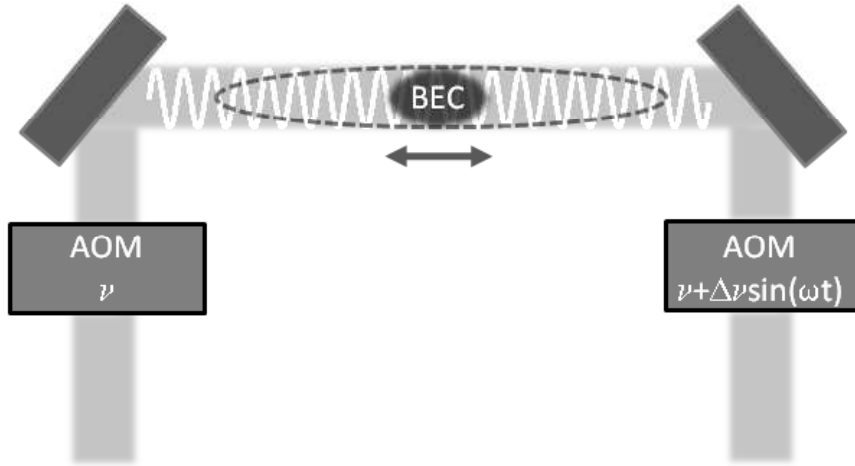


Figure 1.12: Experimental setup for *in-situ* measurement of dynamic localization of a Bose-Einstein condensate (BEC) in a driven optical lattice: The frequencies of two laser beams are shifted with the help of acousto-optic modulators (AOMs) by ν and by $\nu + \Delta\nu \sin(\omega t)$, respectively, before being directed against each other by mirrors. The resulting optical lattice then oscillates in the laboratory frame, giving rise to an oscillating inertial force in the frame of reference co-moving with the lattice. After the initial longitudinal confinement is switched off, the BEC expands by well-to-well tunneling; its final width (indicated by the dashed line) is recorded by imaging its shadow cast by a resonant flash onto a CCD chip. (Figure courtesy of O. Morsch.)

In actual laboratory experiments it is advantageous to work with a phase-coherent atomic Bose-Einstein condensate, rather than with individual atoms: If the density of the condensate is sufficiently low, or if the interatomic *s*-wave scattering length is tuned close to zero by means of a Feshbach resonance [13], the condensate is practically ideal, so that one effectively can perform a measurement on an ensemble of identically prepared noninteracting atoms in a single shot. Figure 1.12 shows a possible experimental setup [3, 4]: The optical lattice is formed by two laser beams of wavelength λ , which are directed against each other with the help of mirrors. Each beam passes through an acousto-optic modulator which shifts its frequency by ν and by $\nu + \Delta\nu(t)$, respectively. Because of the frequency difference $\Delta\nu(t)$ thus introduced between the counterpropagating beams, the condensate experiences the potential

$$V_{\text{lab}}(x, t) = \frac{V_0}{2} \cos \left(2k_L \left[x + \frac{\lambda}{2} \int_0^t d\tau \Delta\nu(\tau) \right] \right) \quad (1.34)$$

in the laboratory frame, which means that the lattice position shifts in time according to the prescribed protocol $\Delta\nu(t)$. In a frame of reference co-moving with the lattice, this shift

translates into the inertial force

$$F(t) = M \frac{\lambda}{2} \frac{d\Delta\nu(t)}{dt} . \quad (1.35)$$

Therefore, choosing $\Delta\nu(t) = \Delta\nu_{\max} \sin(\omega t + \phi)$ leads to the desired Hamiltonian (1.26) in the co-moving frame, with the driving amplitude

$$F_1 = M\omega \frac{\lambda}{2} \Delta\nu_{\max} . \quad (1.36)$$

Now a Bose-Einstein condensate initially trapped in the center of the oscillating lattice is allowed to expand freely in the lattice direction by well-to-well tunneling after switching off the longitudinal confinement, while maintaining a weak transversal confinement in order to keep the condensate in the lattice. After a variable expansion time, the *in situ* width of the condensate is determined by a resonant flash, the shadow cast by which is imaged onto a CCD chip [3]. The measured expansion rate then is to a good approximation proportional to $|J_{\text{eff}}|$, that is, to the absolute value of the effective hopping matrix element (1.12); in principle, even the sign of J_{eff} can be deduced from additional time-of-flight measurements [3]. In Fig. 1.13 we display data for the ratio J_{eff}/J acquired in this manner by the Pisa group with a condensate of ^{87}Rb atoms in a lattice of depth $V_0/E_{\text{rec}} = 6.0$, driven with frequency $\omega/(2\pi) = 4.0$ kHz, after expansion times of 150 milliseconds. Evidently these data match the expected Bessel function $J_0(K_0)$ quite well even up to the second zero. Note that here one has $\hbar\omega/E_{\text{rec}} = 1.24$, so that the frequency employed in these measurements is significantly higher than in our model calculations. This means that the inequality $4J < \hbar\omega$ is satisfied in a stronger manner, while $\hbar\omega$ still remains reasonably small compared to the band gap. As a consequence, even the second band collapse can be quite well developed. In any case, this figure strikingly demonstrates that the concept of dynamic localization by now has crossed, in the context of mesoscopic matter waves, the threshold from an idealized theoretical concept to a well-controllable laboratory reality.

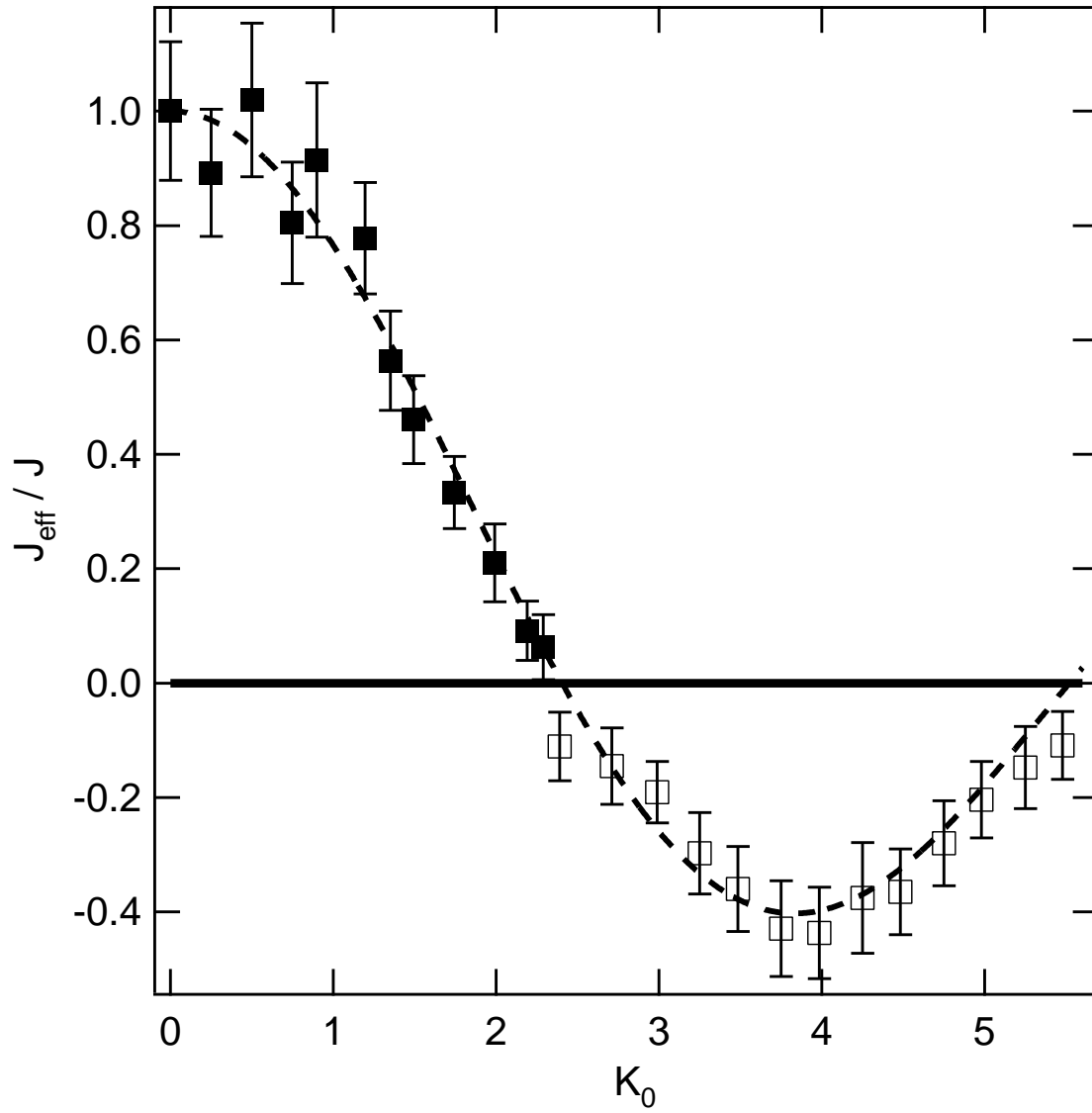


Figure 1.13: Experimental results for the ratio J_{eff}/J of the effective hopping matrix element (1.12) to the bare one as a function of the scaled driving amplitude (1.16), obtained with a Bose-Einstein condensate of ^{87}Rb atoms in an optical lattice with a depth of $V_0 = 6 E_{\text{rec}}$ ($\lambda = 842$ nm), driven with frequency $\omega/(2\pi) = 4.0$ kHz. The dashed line corresponds to the expected Bessel function $J_0(K_0)$. (Figure courtesy of O. Morsch.)

1.3 What is it good for?

Up to this point we have considered no more than a possible realization of dynamic localization which comes fairly close to the theoretical ideal [1]. Apart from its observation with dilute Bose-Einstein condensates in time-periodically shifted optical lattices [3, 4], this type of quantum wave propagation has meanwhile also been made visible by means of an optical analog based on sinusoidally-curved lithium-niobate waveguide arrays [23]. This is certainly interesting, but it is not what one would call “deep”; the “prohibited dephasing”-view clearly reveals that the only physics entering here is summarized by stating that an initial state is “frozen” in time if the phase factors of all of its spectral components evolve at the same speed. Yet, the accompanying band collapse furnishes a strong hint that there may be more in stock. Namely, when the ideal dynamics is somehow perturbed it is the bandwidth which sets the scale with respect to which the strength of such a perturbation has to be gauged. A prominent example is provided by the repulsive interaction between ultracold atoms in an optical lattice; the strength of this interaction is expressed in terms of a parameter U which quantifies the repulsion energy of one pair of atoms occupying the same lattice site [21]. Accordingly, the characteristic dimensionless parameter then is the ratio U/J ; here $J = W/4$ is taken instead of the bandwidth W . Indeed, it is this ratio U/J which decides which quantum phase a gas of ultracold, repulsively interacting atoms in an optical lattice adopts: For $U/J \ll 1$ the system is superfluid, but becomes a Mott insulator when this ratio exceeds a critical value [21]. Hence, when recalling that J is replaced by the effective hopping matrix element (1.12) when the system is driven with appropriate parameters, it is only natural to predict that this superfluid-to-Mott insulator transition can be induced in a time-periodically shifted optical lattice by varying the driving force [24, 25]: Assuming that one starts in the superfluid phase, J_{eff} can then virtually be made arbitrarily small by adjusting the scaled amplitude K_0 to a zero of J_0 , resulting in a value of U/J_{eff} so large that the system is forced to enter the Mott regime. The experimental confirmation of this scenario, achieved by the Pisa group [5], probably constitutes the first known example of coherent control exerted by means of time-periodic forcing on a quantum phase transition.

There are other types of perturbations, associated with deviations from perfect transla-

tional symmetry, which affect even noninteracting ultracold atoms in optical lattices. Most notably, the system governed by the tight-binding Hamiltonian

$$H_{AA} = -J \sum_{\ell} (|\ell + 1\rangle\langle\ell| + |\ell\rangle\langle\ell + 1|) + V \sum_{\ell} \cos(2\pi g\ell + \delta) |\ell\rangle\langle\ell|, \quad (1.37)$$

differing from its antecedent (1.1) through additional on-site energies which oscillate along the lattice with amplitude V , shows a quite peculiar behavior when the number g is irrational, so that this system becomes *quasiperiodic* [26, 27, 28]: As long as $|V/J| < 2$, so that the on-site perturbations are relatively weak, all of its energy eigenstates still remain extended over the entire lattice in a Bloch-like manner, whereas they are all exponentially localized, with one common localization length, when $|V/J| > 2$. Thus, there is a metal-insulator-like, incommensurability-induced transition at $|V/J| = 2$, originally studied by Harper [26] in the context of conduction electrons in a magnetic field, and later by Aubry and André [27]; this transition can be realized approximately with ultracold atoms in a *bichromatic* optical lattice described by the potential

$$V_{\text{bic}}(x) = \frac{V_0}{2} \cos(2k_L x) + V_1 \cos(2gk_L x + \delta). \quad (1.38)$$

The guiding idea here is to employ a primary lattice with depth V_0 for setting up the hosting tight-binding system (1.1), as before, and then to invoke a secondary lattice with much smaller depth $2V_1$ for achieving the required modulation of the local energies at the sites of the host [10, 11]. When the primary lattice is comparatively shallow, possessing a depth of only a few recoil energies, the transition occurs stepwise upon increasing V_1 [12], featuring pronounced mobility edges resulting mainly from the next-to-nearest neighbor couplings between the host's sites which are present in the full bichromatic potential (1.38), but do not occur in the Aubry-André model (1.37). When $V_0/E_{\text{rec}} \gg 1$, so that the primary lattice is so deep that these additional couplings may be safely neglected, the transition occurring in the actual bichromatic lattice (1.38) is fairly sharp. The parameter J then again is given approximately by Eq. (1.25); moreover, one has

$$V/E_{\text{rec}} \sim \frac{V_1}{E_{\text{rec}}} \exp\left(-\frac{g^2}{\sqrt{V_0/E_{\text{rec}}}}\right) \quad \text{for } V_0/E_{\text{rec}} \gg 1 \quad (1.39)$$

with reasonably chosen g on the order of unity. Therefore, the equation $|V/J| = 2$ marking the metal-insulator-like transition in the ideal Aubry-André model now translates into the estimate [12]

$$\frac{V_1^c}{E_{\text{rec}}} \sim \frac{8}{\sqrt{\pi}} \left(\frac{V_0}{E_{\text{rec}}} \right)^{3/4} \exp \left(-2\sqrt{\frac{V_0}{E_{\text{rec}}}} + \frac{g^2}{\sqrt{V_0/E_{\text{rec}}}} \right) \quad (1.40)$$

for the critical strength V_1^c of the secondary optical lattice, given a sufficient depth of the primary one. Indeed, this transition has been observed with a Bose-Einstein condensate consisting of ^{39}K atoms, using a magnetically tunable Feshbach resonance for rendering these atoms practically noninteracting [13].

When ultracold atoms in such a bichromatic lattice (1.38) are subjected to time-periodic forcing, one obtains an additional knob which can be turned to induce the transition: Because J is replaced by the effective hopping strength (1.12) when the system is suitably driven, one can cross the critical border $|V/J_{\text{eff}}| = 2$ by varying the parameters of the driving force; the critical parameters then are linked approximately by the relation

$$|J_0(K_0)| \sim \frac{\sqrt{\pi}}{8} \frac{V_1}{E_{\text{rec}}} \left(\frac{V_0}{E_{\text{rec}}} \right)^{-3/4} \exp \left(+2\sqrt{\frac{V_0}{E_{\text{rec}}}} - \frac{g^2}{\sqrt{V_0/E_{\text{rec}}}} \right). \quad (1.41)$$

Hence, it is feasible to coherently control the metal-insulator-like transition exhibited by noninteracting ultracold atoms in properly designed bichromatic optical potentials through time-periodic forcing [10, 11]. In order to substantiate this prediction, we now display the results of further numerical wave-packet calculations. In all of these we employ a primary lattice with depth $V_0/E_{\text{rec}} = 5.7$, as in our preceding studies, and fix the incommensurability parameter at the golden mean $g = (\sqrt{5} - 1)/2$ up to numerical accuracy. With this choice, the above estimate (1.40) yields $V_1^c/E_{\text{rec}} \approx 0.165$ for the critical strength of the secondary lattice. The driving frequency is given by $\hbar\omega/E_{\text{rec}} = 0.5$ throughout.

Figure 1.14 visualizes the evolution of a wave function that originates from the same Gaussian initial state as already employed in Fig. 1.3. Here the driving force is still absent, and the depth of the secondary lattice is $V_1/E_{\text{rec}} = 0.10$, placing the system in its metallic phase; accordingly, the wave function readily explores the entire lattice. In contrast, when $V_1/E_{\text{rec}} = 0.25$ and the drive is still switched off, the wave function remains localized as shown

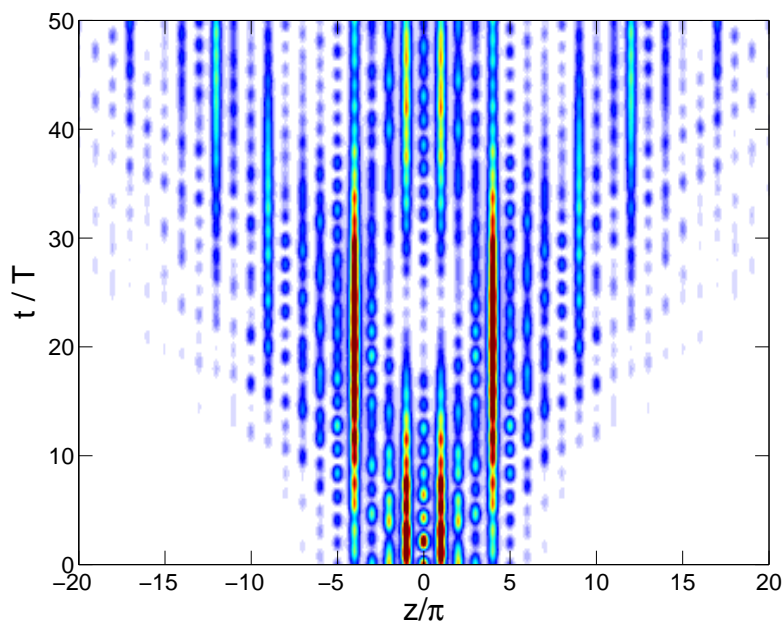


Figure 1.14: Evolution of the same initial wave packet as in Fig. 1.3 in an undriven bichromatic optical lattice (1.38). Here the strength of the secondary potential is $V_1/E_{\text{rec}} = 0.10$, so that the system is in its mobile “metallic” phase, allowing the wave function to spread.

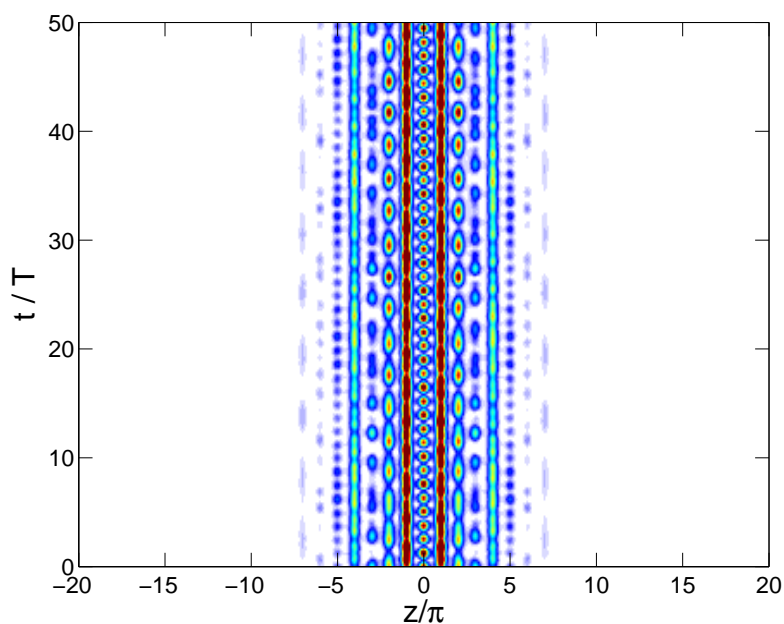


Figure 1.15: Evolution of the same initial wave packet as in Fig. 1.3 in an undriven bichromatic optical lattice (1.38). Here the strength of the secondary potential is $V_1/E_{\text{rec}} = 0.25$, so that the system is in its “insulating” phase, keeping the wave function localized.

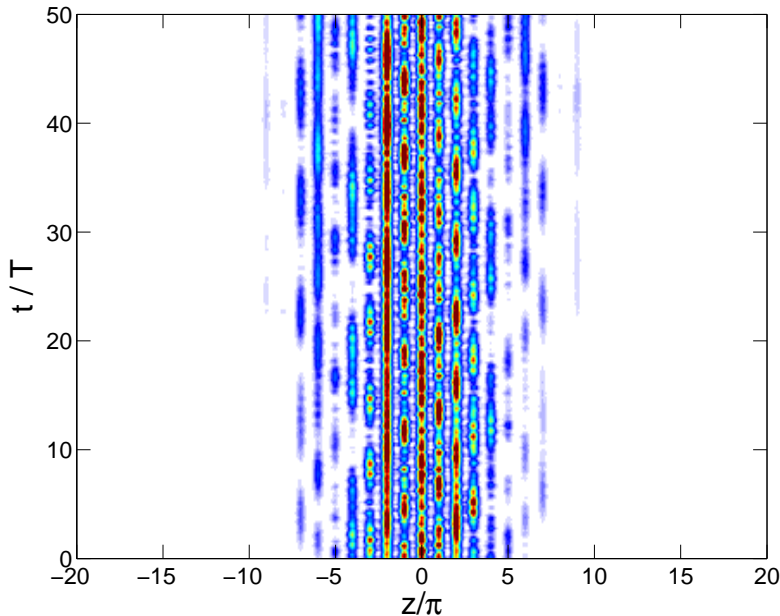


Figure 1.16: Evolution of the same initial wave packet as in Fig. 1.3 in a bichromatic optical lattice (1.38) driven with scaled amplitude $K_0 = 1.7$. The strength of the secondary lattice is $V_1/E_{\text{rec}} = 0.10$, as in Fig. 1.14, so that the system would be in its “metallic” phase if there were no forcing.

in Fig. 1.15; this indicates that we are encountering the insulating phase now. But the wave function also remains localized when the secondary lattice is tuned back to $V_1/E_{\text{rec}} = 0.10$ and the driving force acts with scaled amplitude $K_0 = 1.7$, as depicted in Fig. 1.16: The relation (1.41) predicts the transition from the metallic to the insulating phase to have occurred already at about $K_0 \approx 1.3$. It should be noted that there is a pronounced difference from the ideal dynamic localization reviewed in the preceding section: There the wave packet remains localized only when K_0 is exactly equal to a zero of J_0 . In contrast, here one switches from the metallic into the insulating phase already when $|J_0(K_0)|$ becomes sufficiently small.

Finally, we show a corresponding sequence of results for wave functions which evolve from an initial Wannier state of the primary lattice. In Fig. 1.17 we again consider an undriven bichromatic lattice with $V_1/E_{\text{rec}} = 0.10$, so that the mobile metallic phase enables uninhibited spreading; in Fig. 1.18, where $V_1/E_{\text{rec}} = 0.25$, the system’s insulating character then keeps the wave function strongly localized. But that same high degree of localization may also be obtained when again resetting the strength of the secondary lattice to $V_1/E_{\text{rec}} = 0.10$, and switching on the driving force with scaled amplitude $K_0 = 1.7$, as done in Fig. 1.19.

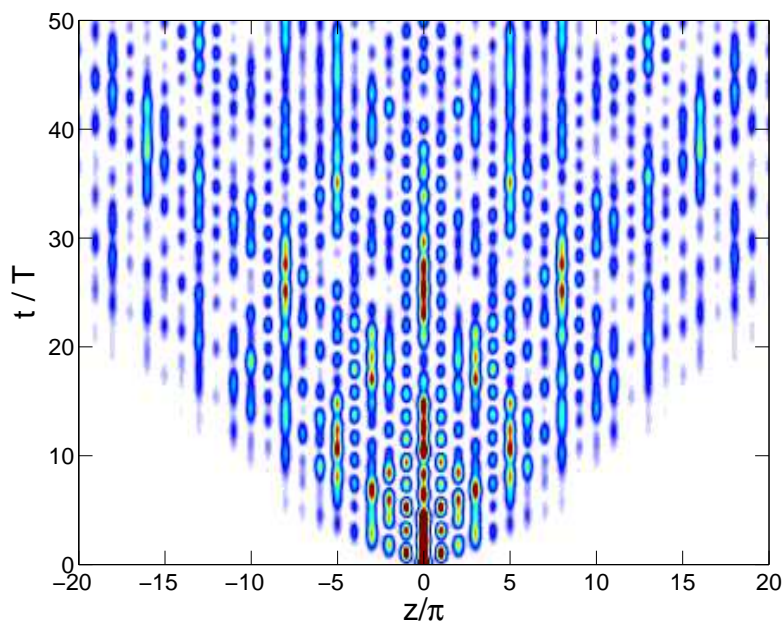


Figure 1.17: Evolution of the wave function originating from a single Wannier state of the primary lattice in an undriven bichromatic optical lattice (1.38). Here the strength of the secondary potential is $V_1/E_{\text{rec}} = 0.10$, so that the system is in its “metallic” phase.

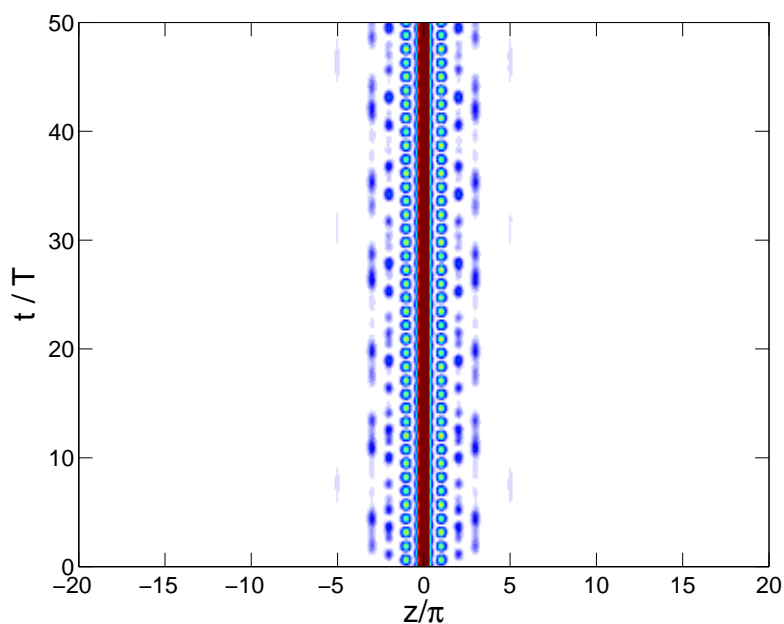


Figure 1.18: Evolution of the wave function originating from a single Wannier state of the primary lattice in an undriven bichromatic optical lattice (1.38). Here the strength of the secondary potential is $V_1/E_{\text{rec}} = 0.25$, so that the system is in its “insulating” phase.

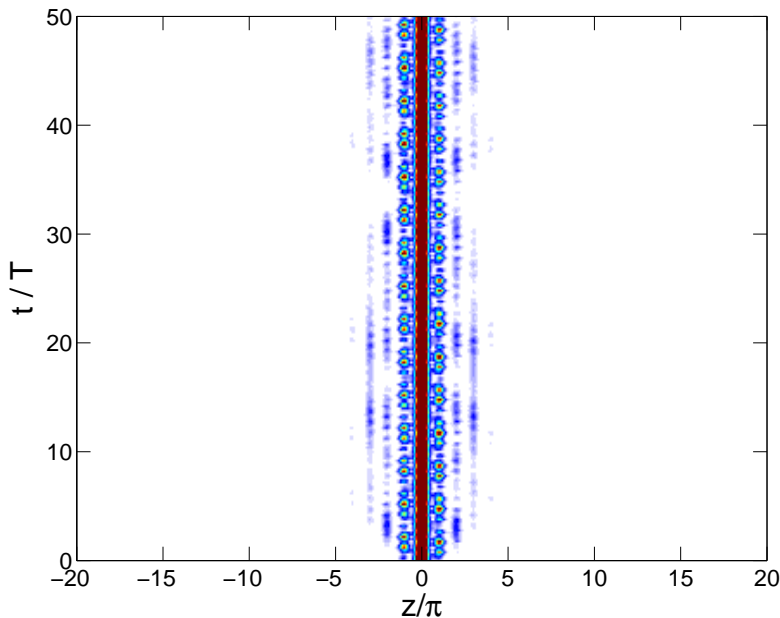


Figure 1.19: Evolution of the wave function originating from a single Wannier state of the primary lattice in a bichromatic optical lattice (1.38) driven with scaled amplitude $K_0 = 1.7$. The strength of the secondary lattice is $V_1/E_{\text{rec}} = 0.10$, as in Fig. 1.17, so that the system would be in its “metallic” phase if there were no forcing.

These figures vividly illustrate the main message: In the presence of time-periodic forcing it is the width of the underlying quasienergy band which determines the effective strength of deviations from perfect spatial periodicity. In an ideal lattice without such deviations one encounters “only” dynamic localization, but in lattices with isolated, quasiperiodic, or random perturbations the strengths of these can be adjusted at will by suitably selecting the parameters of the drive. With regard to experimental tests, the enormous flexibility offered by ultracold atoms in optical potentials makes such systems far superior to electrons in ac-driven crystal lattices.

When the concept of controlling the incommensurability-induced metal-insulator transition exhibited by the Aubry-André model (1.37) by means of time-periodic forcing was conceived [10, 11] the experimental investigation of ultracold atoms in optical lattices was still in its infancies. But now that this transition has been unambiguously observed with a non-interacting Bose-Einstein condensate [13], the demonstration of its coherent control has come into immediate reach. Besides the already established coherent control of the interaction-induced superfluid-to-Mott insulator transition [5], this demonstration would constitute a

further milestone achievement in the on-going effort to explore the newly emerging prospects provided by dressed matter waves.

Acknowledgments

We thank O. Morsch and E. Arimondo for continuing discussions of their experiments [3, 4, 5], and O. Morsch in particular for providing Figs. 1.12 and 1.13. This work was supported by the Deutsche Forschungsgemeinschaft under Grant No. HO 1771/6.

References

- [1] D. H. Dunlap and V. M. Kenkre, “Dynamic localization of a charged particle moving under the influence of an electric field”, *Phys. Rev. B* **34**, 3625-3633 (1986).
- [2] M. M. Dignam and C. M. de Sterke, “Conditions for dynamic localization in generalized ac electric fields”, *Phys. Rev. Lett.* **88**, 046806 (2002).
- [3] H. Lignier, C. Sias, D. Ciampini, Y. Singh, A. Zenesini, O. Morsch, and E. Arimondo, “Dynamical control of matter-wave tunneling in periodic potentials”, *Phys. Rev. Lett.* **99**, 220403 (2007).
- [4] A. Eckardt, M. Holthaus, H. Lignier, A. Zenesini, D. Ciampini, O. Morsch, and E. Arimondo, “Exploring dynamic localization with a Bose-Einstein condensate”, *Phys. Rev. A* **79**, 013611 (2009).
- [5] A. Zenesini, H. Lignier, D. Ciampini, O. Morsch, and E. Arimondo, “Coherent control of dressed matter waves”, *Phys. Rev. Lett.* **102**, 100403 (2009).
- [6] M. Holthaus, “Collapse of minibands in far-infrared irradiated superlattices”, *Phys. Rev. Lett.* **69**, 351-354 (1992).
- [7] M. Holthaus and D. Hone, “Quantum wells and superlattices in strong time-dependent fields”, *Phys. Rev. B* **47**, 6499-6508 (1993).
- [8] D. W. Hone and M. Holthaus, “Locally disordered lattices in strong ac electric fields”, *Phys. Rev. B* **48**, 15123-15131 (1993).

- [9] M. Holthaus, G.H. Ristow, and D.W. Hone, “ac-field-controlled Anderson localization in disordered semiconductor superlattices”, *Phys. Rev. Lett.* **75**, 3914-3917 (1995).
- [10] K. Drese and M. Holthaus, “Ultracold atoms in modulated standing light waves”, *Chem. Phys.* **217** (Special issue: *Dynamics of Driven Quantum Systems*), 201-219 (1997).
- [11] K. Drese and M. Holthaus, “Exploring a metal-insulator transition with ultracold atoms in standing light waves?”, *Phys. Rev. Lett.* **78**, 2932-2935 (1997).
- [12] D. J. Boers, B. Goedeke, D. Hinrichs, and M. Holthaus, “Mobility edges in bichromatic optical lattices”, *Phys. Rev. A* **75**, 063404 (2007).
- [13] G. Roati, C. D’Errico, L. Fallani, M. Fattori, C. Fort, M. Zaccanti, G. Modugno, M. Modugno, and M. Inguscio, “Anderson localization of a non-interacting Bose-Einstein condensate”, *Nature* **453**, 895-898 (2008).
- [14] W. V. Houston, “Acceleration of electrons in a crystal lattice”, *Phys. Rev.* **57**, 184-186 (1940).
- [15] J. H. Shirley, “Solution of the Schrödinger equation with a Hamiltonian periodic in time”, *Phys. Rev.* **138**, B979-B987 (1965).
- [16] Ya. B. Zel’dovich, “The quasienergy of a quantum-mechanical system subjected to a periodic action”, *Zh. Eksp. Theor. Fiz.* **51**, 1492-1495 (1966) [*Sov. Phys. JETP* **24**, 1006-1008 (1967)].
- [17] V. I. Ritus, “Shift and splitting of atomic energy levels by the field of an electromagnetic wave”, *Zh. Eksp. Theor. Fiz.* **51**, 1544-1549 (1966) [*Sov. Phys. JETP* **24**, 1041-1044 (1967)].
- [18] H. Sambe, “Steady states and quasienergies of a quantum-mechanical system in an oscillating field”, *Phys. Rev. A* **7**, 2203-2213 (1973).
- [19] S. Arlinghaus and M. Holthaus, “Driven optical lattices as strong-field simulators”, *Phys. Rev. A* **81**, 063612 (2010).
- [20] O. Morsch and M. Oberthaler, “Dynamics of Bose-Einstein condensates in optical lattices”, *Rev. Mod. Phys.* **78**, 179-215 (2006).
- [21] I. Bloch, J. Dalibard, and W. Zwerger, “Many-body physics with ultracold gases”, *Rev. Mod. Phys.* **80**, 885-964 (2008).
- [22] N. W. Ashcroft and N. D. Mermin, “Solid state physics”, Harcourt College Publishers, Fort Worth, 1976 (see chapter 12 therein).

- [23] S. Longhi, M. Marangoni, M. Lobino, R. Ramponi, P. Laporta, E. Cianci, and V. Foglietti, “Observation of dynamic localization in periodically curved waveguide arrays”, *Phys. Rev. Lett.* **96**, 243901 (2006).
- [24] A. Eckardt, C. Weiss, and M. Holthaus, “Superfluid-insulator transition in a periodically driven optical lattice”, *Phys. Rev. Lett.* **95**, 260404 (2005).
- [25] C. E. Creffield and T. S. Monteiro, “Tuning the Mott transition in a Bose-Einstein condensate by multiple photon absorption”, *Phys. Rev. Lett.* **96**, 210403 (2006).
- [26] P. G. Harper, “Single band motion of conduction electrons in a uniform magnetic field”, *Proc. Phys. Soc. A* **68**, 874-878 (1955).
- [27] S. Aubry and G. André, “Analyticity breaking and Anderson localization in incommensurate lattices”, *Ann. Israel Phys. Soc.* **3**, 133-140 (1980).
- [28] J. B. Sokoloff, “Unusual band structure, wave functions and electrical conductance in crystals with incommensurate periodic potentials”, *Phys. Rep.* **126**, 189-244 (1985).